A nucleoid-associated protein is involved in the emergence of antibiotic resistance by promoting the frequent exchange of the replicative DNA polymerase in *M. smegmatis*

Wei L. Ng [a], Jin Ho Park [a], and E. Hesper Rego[1] [a]

Affiliations

[a] Department of Microbial Pathogenesis, Yale University School of Medicine, New Haven, CT 06519

[1]To whom correspondence should be addressed: hesper.rego@yale.edu

SUMMARY

Antibiotic resistance in *M. tuberculosis* exclusively originates from chromosomal mutations, either during normal DNA replication or under stress, when the expression of error-prone DNA polymerases increases to repair damaged DNA. The mechanisms by which polymerases switch at the replication fork are unknown. Here, we discover that a mutation in the nucleoid-associated protein, Lsr2, produces several hallmarks of an impaired DNA damage response, including a severe growth defect when exposed to genotoxic drugs and reduced mutation frequency. Lsr2's function as a transcription factor cannot explain these phenotypes. Instead, through a series of genetic and fluorescence imaging experiments, we find that Lsr2 is important for modulating the dynamics of polymerases at the replication fork. The major replicative DNA polymerase, DnaE1, exchanges more frequently in the presence of Lsr2, while, during DNA damage, cells lacking *lsr2* cannot effectively load the complex needed to bypass DNA lesions, and thus replicate with higher fidelity but exhibit growth defects. Together, our results show that

Lrs2 promotes dynamic flexibility of the mycobacterial replisome, which is critical for robust cell growth and lesion repair in conditions that damage DNA.

INTRODUCTION

DNA replication and repair are fundamental to bacterial evolution. The function of DNA replication and repair pathways are key determinants of the balance between genetic stability and mutability. To establish this balance, bacteria encode and regulate numerous DNA polymerases with specialized functions in different conditions (1). Importantly, the emergence of antibiotic resistance in the major human pathogen *M. tuberculosis* is mainly driven by chromosomal mutagenesis, as *M. tuberculosis* has little to no ability for horizontal gene transfer (2, 3). Furthermore, numerous studies suggest a critical role for *de novo* mutagenesis and differences in mutation rates underlie the emergence of *M. tuberculosis* drug resistance (4, 5, 6, 7, 8). Thus, the mechanisms regulating polymerase expression and activity are of particular importance in mycobacterial evolution.

In mycobacteria, the fidelity of chromosome replication is established by the major replicative polymerase DnaE1, which possesses endogenous proofreading activity (9). In addition to DnaE1, mycobacteria encode a suite of other polymerases with specialized repair functions that are only expressed under certain conditions, such as oxidative or DNA-damaging stress (10, 11, 12). For example, the mycobacterial specialist polymerases DinB1, DinB2, DinB3, and DnaE2 are induced under different conditions and have varying repair activities and mutational signatures (10, 11, 12, 13, 14, 15). Of particular importance is the error-prone polymerase DnaE2. It and its accessory proteins ImuA' and ImuB, collectively referred to as the 'mutasome', are highly expressed in conditions that damage DNA and are the primary drivers of stress-induced mutagenesis *in vitro* and potentially *in vivo* (10, 11, 16). In general, however, the

47 mechanisms that facilitate switching between polymerases at the site of repair are not well
48 understood, especially in mycobacteria (17).

49 As in *E.coli*, the abundance and function of the proteins involved in DNA repair are
50 tightly regulated transcriptionally and proteolytically in mycobacteria (18, 19, 20, 21). At the
51 transcriptional level, mycobacteria encode two stress-inducible DNA repair pathways: the
52 canonical SOS response, which is jointly controlled by transcriptional repressor LexA and co-
53 protease RecA, and an independent, Actinobacteria-specific response controlled by the
54 transcriptional activator PafBC (22, 23, 24, 25). Both pathways regulate the expression of
55 mycobacterial mutasome in *M. smegmatis* and in *M. tuberculosis* (25). DNA replication and
56 repair machinery are also regulated post-translationally in mycobacteria. For example, RecA
57 activity is controlled by post-translational modification, and RecA protein is targeted for
58 degradation to the Pup-proteasome system (23, 26). Studies from *E. coli* also suggest
59 additional, more complex mechanisms of regulating mutagenesis, including spatial
60 sequestration of key proteins, replisome dynamics, collisions with transcription complexes, and
61 complex expression dynamics at the single-cell level (18, 19, 20, 21, 27, 28, 29, 30, 31).
62 Discovery of similar mechanisms is starting to emerge from studies in mycobacteria. For
63 example, RecA fluctuates dynamically and heterogeneously in single genetically identical *M.*
64 *tuberculosis* cells, and the DNA translocase Mfd promotes mutagenesis in *M. tuberculosis* and
65 many other bacteria, possibly through transcription-associated mutagenesis (27, 32, 33).
66 Furthermore, the distinct localization patterns of the mycobacterial DnaE2/ImuA'/ImuB
67 translesion DNA polymerase complex members indicate potential spatial regulation (34).

68 Here, we decided to investigate the expression of ImuA' and ImuB, encoded by a single
69 operon, *imuA'B*, at the single cell level by creating fluorescence reporters that could be used to
70 measure their expression by flow cytometry and microscopy. We serendipitously discovered a
71 mutant in the Actinobacteria-specific nucleoid-associated protein Lsr2 that resulted in higher

72 fluorescence, and several phenotypes associated with dysregulation of the DNA-damage
73 response (35). However, by analyzing both endogenous *imuA'B* expression and expression
74 from synthetic constructs, we demonstrate that Lsr2 regulation of the *imuA'B* promoter is
75 counteracted by the addition of neighboring sequences. Thus, our data indicate that Lsr2 has a
76 limited effect on the transcriptional regulation of *imuA'B.* Instead, using fluorescence imaging
77 techniques, including fluorescence recovery after photobleaching (FRAP), we discover that Lsr2
78 has a novel role in modulating the dynamics of the replisome and exchange of polymerases
79 within. Specifically, in cells missing *lsr2,* DnaE1 exchanges with the cytoplasmic pool more
80 slowly, and ImuB exchanges more quickly, suggesting ineffective loading of the mutasome.
81 Consistently, loss of *lsr2* results in growth defects in conditions that damage DNA, and reduced
82 mutagenesis. Overall, our data provide another unexpected layer to the mechanisms
83 mycobacteria use to mutate and acquire drug resistance.

84

85 **RESULTS**

86 **Lsr2 affects the levels of an *imuA'B* promoter reporter, growth in mitomycin, and**
87 **acquisition of mutations**

88 To investigate the expression of the mutasome in single cells, we constructed
89 fluorescent reporters for *dnaE2* and *imuA'B* promoter activity by fusing 500 bp upstream of the
90 start codon to a promoterless GFP (*pimuAB-msfGFP*) or mScarlet (*pdnaE2-mScarlet*) (**Fig 1A**).
91 We integrated these reporters in single copy at phage sites on the *M.smegmatis* chromosome.
92 *imuA'B* and *dnaE2* are induced upon exposure to DNA-damaging agents and are controlled by
93 several transcription factors (23, 25). To verify that our fusions were responsive to these
94 elements, we first exposed cells to the DNA-damaging agent mitomycin C (MMC, 80 ng/ml), and
95 observed the expected increase in reporter fluorescence by flow cytometry (**Fig 1B**). Given the

96 complex regulation associated with *imuA'B* expression, we focused on its single-cell distribution
97 in strains altered for the transcriptional regulators LexA and PafBC. As *lexA* is essential in
98 mycobacteria, we used CRISPRi to deplete *lexA* levels and monitored reporter fluorescence
99 (36, 37, 38). Consistent with LexA's function as a repressor, *lexA* knockdown increased the
100 average fluorescence of the population under basal conditions. Additionally, we observed little
101 to no change in fluorescence upon *lexA* depletion during MMC treatment, which is consistent
102 with the cleavage of LexA protein under these conditions (**Fig 1C**). Some DNA damage
103 response genes, including *imuA'B*, are transcriptionally activated by PafBC when exposed to

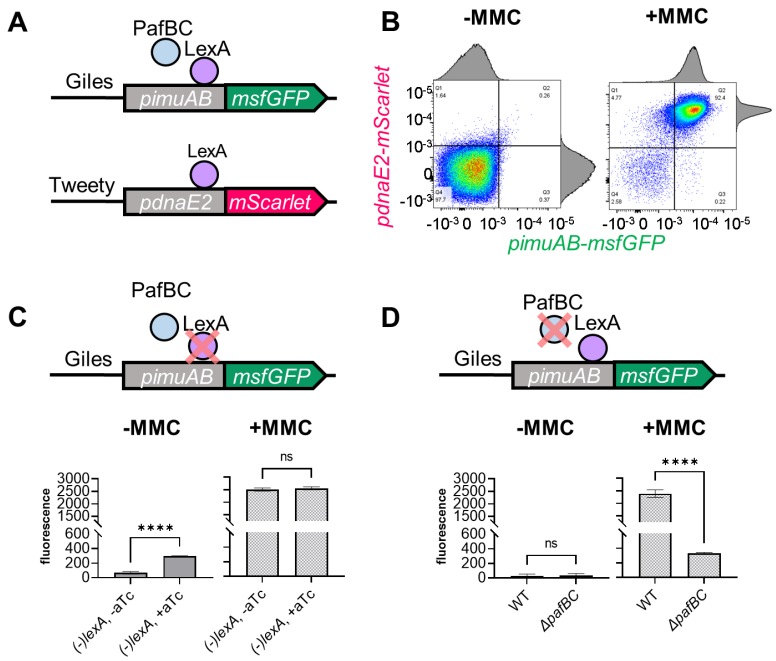

FIG 1. Construction & evaluation of *imuA'B* promoter fusion. (A) Schematic illustrating the design of *imuA'B* and *dnaE2* fluorescent promoter fusions on phage integrative vectors. Transcriptional regulators LexA and PafBC are also shown. **(B)** Representative flow cytometry plot of a strain harboring the *imuA'B* and *dnaE2* promoter fusions. DNA damage was induced by adding mitomycin C (MMC) (80 ng/ml, 6 hours). **(C,D)** Mean (±SD) of the median fluorescence intensities obtained from flow cytometry (N=3 biological replicates) in a *pimuAB-msfGFP* expressing strain with or without aTc-inducible CRISPRi knockdown of *lexA* **(C)** *or pafBC* **(D)**. DNA damage was induced by mitomycin C treatment (80 ng/ml, 11 hours). *lexA* knockdown was induced by adding aTc (11-12 hours, 100 ng/ml) prior to mitomycin C treatment. For all panels: p-values were obtained by unpaired t-test. 0.1234 (ns), 0.0332 (*), 0.0021 (**), 0.0002 (***), <0.0001 (****).

104

105 DNA damaging agents (23). PafBC is present but inactive in basal conditions, and becomes
106 activated during DNA damage (39). Consistently, deletion of *pafBC* resulted in little to no
107 change in fluorescence under basal conditions. In contrast, under DNA-damaging conditions,
108 cells missing *pafBC* had 6-fold lower fluorescence than wild-type cells (**Fig 1D**). Together, these
109 results show that our fluorescence reporter is responsive to known regulatory elements within
110 the promoter of *imuA'B*.

111 In subsequent studies, we observed the spontaneous emergence of a subpopulation
112 with dramatically higher levels of *imuA'B* promoter reporter fluorescence. We performed whole
113 genome sequencing to identify mutations exclusively found in clones that exhibited higher
114 fluorescence. Notably, all three isolates with elevated fluorescence had a smooth colony
115 morphology and contained inactivating mutations in the nucleoid-associated protein *lsr2*
116 (MSMEG_6092), which were absent from the three isolates with a rough colony morphology
117 and comparatively low fluorescence. To confirm that *lsr2* inactivation is responsible for elevated
118 *imuA'B* promoter reporter fluorescence, we generated a clean *lsr2* deletion mutant by
119 recombineering (40). As expected, Δ*lsr2* exhibited higher reporter fluorescence under both
120 basal and DNA damaging conditions, which could be complemented by expressing *lsr2* from the
121 native promoter on a phage integrated plasmid (**Fig 2A**).

122 Despite extensive research into transcriptional regulation by Lsr2, no previous reports
123 have shown Lsr2 regulation of *imuA'B* or other DNA damage response genes (41, 42, 43, 44).
124 Therefore, we further validated this observation of Lsr2 regulation of *imuA'B* by replacing the
125 chromosomal copy of *imuA'B* with *msfGFP* using recombineering, effectively recreating the
126 p*imuAB* reporter at the native locus. We performed flow cytometry of this reporter in a wild-type
127 and Δ*lsr2* background. As with the reporter integrated at the phage integration site, cells
128 expressing the fluorescent protein at the native locus also exhibited higher fluorescence in the
129 absence of *lsr2* (**Fig 2B**). Importantly, ImuA' or ImuB themselves were not responsible, as

130 reporter fluorescence increased regardless of their expression (**Fig S1**). Together, these results

131 show that Lsr2 regulates p*imuAB* reporter fluorescence.

132 *M. smegmatis* and *M. tuberculosis* cells missing ImuA' and ImuB are more sensitive to

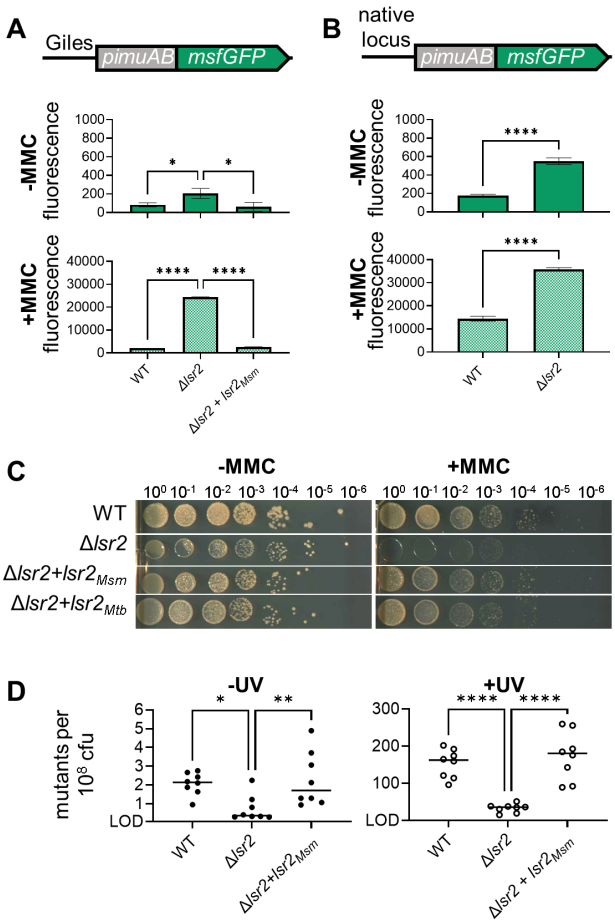

FIGURE 2. Loss of *lsr2* leads to increased reporter fluorescence, growth defects on mitomycin C, and decreased mutagenesis. (A) Mean (±SD) of the median fluorescence intensities obtained from flow cytometry data (N=3) in a strain expressing *pimuAB-msfGFP* from the Giles *attB* site in either a wild-type or Δ*lsr2* background. DNA damage was induced by mitomycin C treatment (80 ng/ml, 9 hours). **(B)** Mean (±SD) of the median fluorescence intensities obtained from flow cytometry data (N=5) in a strain expressing *pimuAB-msfGFP* from the *imuAB* locus in either a wild-type or Δ*lsr2* background. DNA damage was induced by mitomycin C treatment (80 ng/ml, 7 hours). **(A-B)** p-values were obtained by unpaired t-test. **(C)** Serial dilutions of WT, Δ*lsr2*, and complemented strains on agar plates with or without mitomycin C (1.56 ng/ml). Results shown are representative spots of biological triplicates. **(D)** Frequency of rifampin-resistant mutants per 10^8 cfu without or with UV-induced DNA damage (20 mJ/cm^2). LOD refers to the limit of detection. *lsr2* complements were expressed from the native *lsr2* promoter on a phage integrative plasmid. p-values were obtained by one-way ANOVA. For all panels: 0.1234 (ns), 0.0332 (*), 0.0021 (**), 0.0002 (***), <0.0001 (****).

133 MMC treatment and are less likely to mutate when exposed to DNA-damaging agents, like
134 ultraviolet light (**Fig S2**) (16, 34). As our data indicated that Lsr2 is involved in the transcription
135 of *imuA'B*, we hypothesized that cells missing *lsr2* would be altered in these key phenotypes. To
136 test this, we first grew cells on agar plates with different concentrations of MMC. Deletion of *lsr2*
137 results in a severe growth defect in the presence of MMC (**Fig 2C**). Next, we assayed the ability
138 of Δ*lsr2* to acquire resistance to rifampicin, both spontaneously and when exposed to UV. We
139 chose a dose of UV that resulted in no survival difference between the two genotypes (**Fig S3**).
140 Consistent with a role in DNA damage response, we found that cells deleted for *lsr2* are
141 approximately 4-5 times less likely to acquire resistance to rifampicin when exposed to UV (**Fig**
142 **2C, right**). In addition, Δ*lsr2* is less likely to spontaneously acquire resistance, suggesting that
143 Lsr2's role is not strictly limited to conditions that induce DNA damage (**Fig 2C, left**). Taken
144 together, our data indicate a role for Lsr2 in promoting cellular growth during DNA damage and
145 the acquisition of mutations that confer drug resistance.

146

147 **RNAseq reveals a discrepancy between promoter reporter fluorescence and endogenous**
148 **RNA levels for many DNA-damage associated genes**

149 Lsr2 is a nucleoid-associated protein that is conserved in mycobacteria and related
150 actinomycetes (35, 42, 45, 46, 47). Like H-NS in *E.coli*, Lsr2 primarily binds AT-rich regions of
151 DNA and functions as a global transcriptional repressor (35). Notably, *in vitro* studies show that
152 Lsr2 binding interferes with transcription, inhibits topoisomerase I-dependent supercoil
153 relaxation, and protects DNA from DNase I digestion and H2O2-mediated degradation (42).
154 Loss of *lsr2* is associated with a wide range of different phenotypes in mycobacteria, including
155 altered cell cycle timing, and growth defects upon entering/exiting hypoxic conditions and when
156 exposed to oxidative stress and various antibiotics (41, 42, 43, 44, 48). Lsr2 is also involved in
157 resistance against phage infection, protection against reactive oxygen intermediates during

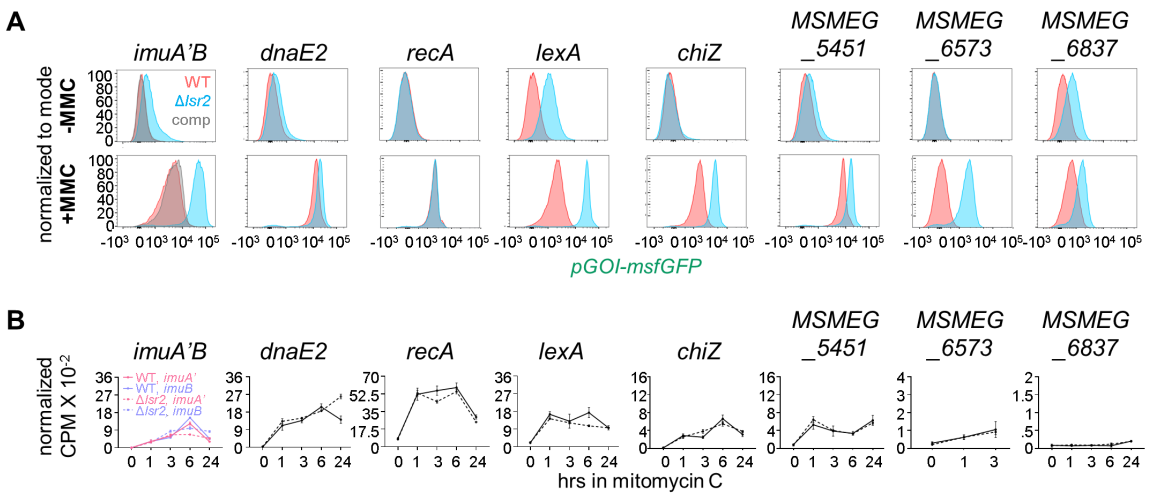

FIGURE 3. RNA-seq reveals a discrepancy between reporter fluorescence and endogenous RNA levels for many DNA damage-associated genes. (A) Flow cytometry histograms of strains expressing various DNA-damage inducible promoter reporters from the Giles *attB* site in either a wild-type (red) or Δ*lsr2 (*blue) background. *M. smegmatis lsr2* complement (grey) was expressed from the native promoter at the Tweety *attB* site. DNA damage was induced by mitomycin C treatment (80 ng/ml, 9 hours). **(B)** Normalized counts per million (mean ±SD) for different DNA-damage inducible genes over time in either wild-type (solid line) and Δ*lsr2* (dashed line). In the *imuAB* plot, *imuA* and *imuB* RNA levels are shown in pink and purple, respectively. None of the genes shown were differentially expressed in Δ*lsr2* compared to WT (|log2FC|>1, p<0.05). DNA damage was induced by mitomycin C treatment (80 ng/ml).

158 macrophage infection, and cells deleted for *lsr2* show reduced virulence in various hosts,
159 including mice (41, 44, 46, 49).

160 We set out to understand the molecular basis of Lsr2's role in promoting growth in
161 conditions that damage DNA and in acquiring mutations. As our data indicated a change in
162 *imuA'B* promoter activity in Δ*lsr2*, we hypothesized that Lsr2 acts as a transcription factor to
163 control the expression of proteins important for repairing DNA. Prior studies on role of Lsr2 in
164 gene expression under aerobic growth conditions as well as exposure various stressors,
165 including ethambutol, hypoxia, and hydrogen peroxide, did not report differential expression of
166 *imuA'B* or related genes, including *recA, dnaE2,* and *lexA,* in Δ*lsr2* (41, 42, 43, 44). We
167 hypothesized that lack of differential expression of DNA damage genes could be due to the lack

168 of or insufficient DNA damage induction in the conditions used. We therefore performed RNA-
169 seq at different time points throughout treatment with mitomycin C, a strong DNA damage
170 inducer. Consistent with previous studies, we observed up-regulation of many cell envelope
171 biosynthesis genes in basal conditions, including MSMEG_4727, in Δ*lsr2* (43) (**Tables S3 and**
172 **S4**). Curiously, although our *imuA'B* promoter reporter showed higher levels of fluorescence and
173 *msfGFP* RNA in the *lsr2* mutant background (**Fig 2A, 2B, 4C**), RNA-seq and RT-qPCR showed
174 that *imuA'* and *imuB* mRNA levels were either similar or slightly lower in Δ*lsr2* than in wild type
175 (**Tables S3 and S4**, **Fig 4A**). To examine whether the discrepancy between the promoter
176 reporter and endogenous RNA levels was generalizable to other DNA damage-inducible genes,
177 we constructed phage site-integrated fluorescent promoter reporters for several other DNA-
178 damage inducible genes. Of the seven additional reporters we constructed, five showed
179 increased fluorescence in the *lsr2* mutant background compared to wild type in the presence
180 and/or the absence of MMC (**Fig 3A**)**.** As seen with *imuA'B,* RNA-seq data showed little to no
181 difference in endogenous mRNA levels in Δ*lsr2* compared to wild type in in the absence of MMC
182 or at any timepoint ranging from 1 to 24 hours of treatment (**Fig 3B**). Taken together, these data
183 show that *lsr2* exhibits repression of promoter reporter constructs, even those integrated at the
184 native locus, but has little to no effect on endogenous RNA levels, suggesting that DNA outside
185 the promoter region contributes to gene expression.

186

187 **Sequence context is important for regulation of *imuA'B***

188 *lsr2* represses the expression of promoter reporters for multiple DNA damage-inducible
189 genes, but has little to no effect on endogenous RNA levels (**Fig 3A**). We thus hypothesized
190 that DNA outside the promoter region contribute to gene expression. In fact, when we carefully
191 looked at the RNA-seq reads mapped to the *imuA'B* locus, we noticed a high number of
192 antisense reads mapped to the 3' region of *imuA'B* (**Fig 4B**). The coding sequence of this region

193 includes *iunH,* which is predicted to encode a nucleoside hydrolase (50). The architecture of
194 *imuA'B-iunH* is conserved across mycobacterial species (24). Indeed, prior studies in *M.*
195 *tuberculosis* using microarrays, which cannot distinguish strandedness, noticed a high number
196 of *iunH* reads when *M. tuberculosis* was exposed to MMC (24). The expression of transcripts
197 depended on the presence of *recA* despite the absence of an SOS box in the promoter region of
198 *iunH*. Thus, the authors speculated the presence of anti-sense RNA in this region. We
199 wondered if the presence of this RNA was the result of transcriptional readthrough from *imuA'B*,
200 or if there existed an internal promoter within *imuA'B* driving expression. To distinguish these
201 two possibilities, we designed primers for the *imuB-iunH* junction, and performed quantitative
202 real-time PCR (**Fig S4A, S4B**). Consistent with transcriptional readthrough, we observed high
203 levels of this product in the reaction. Second, we fused the *imuA'B* coding region to a
204 promoterless GFP, and did not observe fluorescence in the absence or presence of MMC,
205 suggesting that *imuA'B* does not harbor an internal promoter (**Fig S4C**). Together, these data
206 suggest that the antisense *iunH* reads most likely originate from transcriptional readthrough of
207 *imuA'B*, and the *imuA'B* transcript includes a large 3' UTR, which is conserved in *M.*
208 *tuberculosis* (24).

209 We hypothesized that additional regulation originating from this 3' region is responsible
210 for the discrepancy between our promoter fusion and transcript abundance. To test this, we
211 added 1.55kb sequence downstream of *imuB* to the 3' end of the *msfGFP* coding sequence of
212 our reporter and measured *msfGFP* transcript abundance by RT-qPCR. This 1.55kb
213 downstream sequence includes the *iunH* coding sequence and 500 additional bases to account
214 for *iunH* upstream regulatory elements. Consistent with our hypothesis, we observed that
215 transcript levels were more similar between wild type and Δ*lsr2* cells when we added the
216 downstream region (**Fig 4C**). Specifically, we noticed that when we added the downstream
217 region, *msfGFP* transcript levels in wild type increased to a level similar to those in *Δlsr2*. To

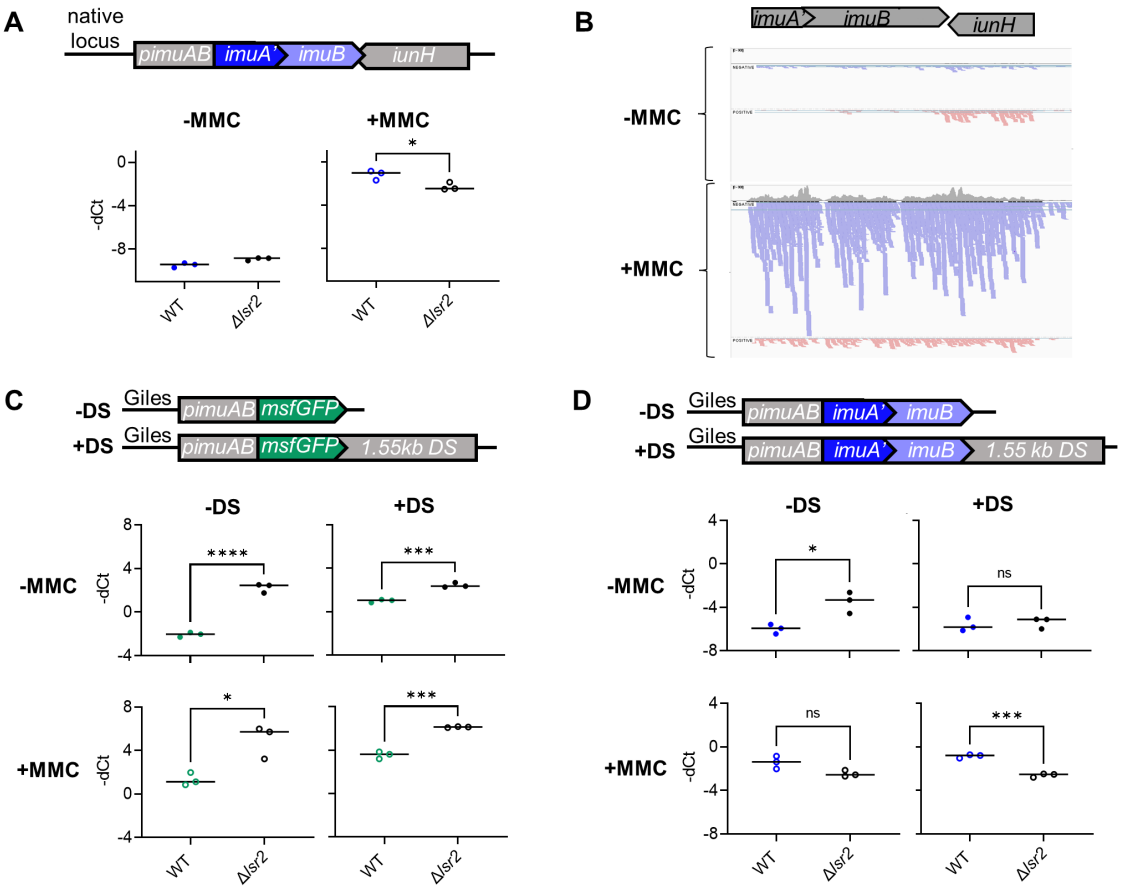

FIGURE 4. Lsr2 regulation of the *imuA'B* promoter is counteracted by the addition of neighboring sequences. (A) RT-qPCR of endogenous *imuA* RNA. **(B)** RNA-seq reads at the *imuA'B* locus visualized in IGV. Top strand (blue), bottom strand (red). DNA damage was induced by mitomycin C treatment (80 ng/ml, 6 hours). **(C, D)** Schematic and RT-qPCR of *msfGFP* or *imuA'* from phage integrative constructs. +/- DS indicates the presence or absence of a 1.55kb region (including the *iunH* coding sequence) downstream the *imuB* coding sequence. **(A, C, D)** Results shown are the median -dCt values of biological triplicates, with individual values shown as dots. Larger -dCt values correspond to higher expression. Phage integrative constructs in **(C)** and **(D)** are expressed in a WT and Δ*imuAB* background, respectively. DNA damage was induced by mitomycin C treatment (80 ng/ml, 9 hours). p-values were obtained by unpaired t-test. 0.1234 (ns), 0.0332 (*), 0.0021 (**), 0.0002 (***), <0.0001 (****).

confirm that this also true for a transcript that includes the coding sequence of *imuA'B*, instead of *msfGFP*, we integrated constructs containing the *imuA'B* coding sequence in cells deleted for *imuA'B*, and performed RT-qPCR (**Fig 4D**). In this case, the effect of the downstream region was much smaller, pointing to important elements within the coding sequence itself.

223 Nevertheless, the only scenario that recapitulated the levels of endogenous mRNA as
224 measured by the RNA-seq in both basal and MMC conditions included the region 3' to *imuA'B*.
225 Together these data show that regulatory or structural elements within the coding sequence and
226 the 3' region adjacent to *imuA'B* are responsible for the discrepancy between our promoter
227 fusion and RNA-seq data. Specifically, these data suggest that Lsr2 is capable of strongly
228 regulating the promoter of *imuA'B*, directly or indirectly, but does not when these other genomic
229 elements are present. One possible interpretation is that the coding sequence and adjacent 3'
230 region of the DNA forms a local DNA structure that is propagated to the promoter region and
231 prevents Lsr2 regulation. Although it is not clear whether Lsr2 directly regulates p*imuAB-GFP*
232 transcription certain NAPs are thought preferentially bind locally deformed DNA (51, 52, 53).
233 Notably, transcriptional regulation of the *proU* operon by *Salmonella typhimurium* H-NS also
234 depends on the sequence context (54).

235

236 **Tn-seq reveals a connection between Lsr2 and stalled transcription complexes**

237 Our data show that while the promoter of *imuA'B* may be responsive to Lsr2 in some
238 contexts, other factors are more important in controlling the endogenous levels of this transcript.
239 More broadly, we could not detect any change in the expression of genes known to be important
240 for DNA repair or replication in Δ*lsr2* in our RNA-seq data (**Tables S3 and S4**). Thus, we
241 conclude that Lsr2's function as a transcription factor is unlikely to account for its role in
242 surviving DNA damage survival and acquiring mutations.

243 Why, then, does Δ*lsr2* display phenotypes associated with dysregulation of the DNA-
244 damage response? Specifically, cells missing *lsr2* display some phenotypes typically associated
245 with cells missing DnaE2, the major error-prone polymerase, or its accessory proteins, ImuA'
246 and ImuB, despite having similar amounts of these transcripts (16). We reasoned that changes

#Orf	Name	Description	log2FC	Adj. p-value
MSMEG_3437c	-	putative esterase family protein	-6.17	0
MSMEG_6642	-	caib/baif family protein	-6.1	0
MSMEG_6136c	-	membrane protein, TerC family protein	-5.65	0
MSMEG_2107	-	hypothetical protein MSMEG_2107	-5.52	0
MSMEG_5089	-	hypothetical protein MSMEG_5089	-5.46	0
MSMEG_6230c	-	acyltransferase	-5.3	0
MSMEG_3186c	glgX	glycogen debranching enzyme GlgX	-5.21	0
MSMEG_5534c	**pcrA**	**ATP-dependent DNA helicase PcrA**	**-5.06**	**0**
MSMEG_0641c	-	binding-protein-dependent transport systems inner membrane component	-5.05	0
MSMEG_0167c	-	transmembrane transport protein	-4.8	0
MSMEG_6768c	-	halogenase	-4.73	0
MSMEG_3225	-	ferredoxin-dependent glutamate synthase 1	-4.49	0
MSMEG_2174	**-**	**superfamily protein I DNA or RNA helicase**	**-4.38**	**0**
MSMEG_1222c	-	ISMsm6, transposase	-4.28	0
MSMEG_4038	-	vanillin dehydrogenase	-4.21	0
MSMEG_2263	hybC	hydrogenase-2, large subunit	-4.07	0
MSMEG_0147c	-	C-5 sterol desaturase	-4.06	0
MSMEG_1219c	-	ABC-type transport system permease protein II	-4.04	0
MSMEG_5942c	-	AMP-dependent synthetase and ligase	-3.76	0
MSMEG_0816c	-	flavin-binding monooxygenase	-2.81	0
MSMEG_0408c	-	type I modular polyketide synthase	-2.04	0
MSMEG_5571c	-	ABC transporter ATP-binding protein	-6.73	0.0192

Table 1. Differential abundance of transposon mutants in a Δ*lsr2* library compared to wild-type. Light green shading corresponds to two genes harboring UvrD-like helicase domains that are substantially less abundant in Δ*lsr2* than wild-type.

247 in

248 gene essentiality might reveal additional cellular pathways associated with Lsr2 function. To that

249 end, we used Tn-seq to map essential pathways in cells with and without Lsr2. Of the 20 genes

250 that had the most significantly reduced transposon insertions in the mutant, many coded for

251 proteins involved in cell wall synthesis, consistent with Lsr2's function as a mediator of cell wall

252 composition of *M.smegmatis*. However, two genes with significantly fewer insertions contained

253 UvrD-like helicase domains, including HelD, which promote RNAP recycling at sites of stalled

254 transcription complexes (**Table 1**) (55). In bacteria, head-on collisions between transcription and

255 replication complexes can be lethal if not resolved (31). Thus, our Tn-seq data indicate that

256 replication/transcription collisions may occur more frequently or are less resolved in cells
257 missing *lsr2*. Along these same lines, Lsr2 inhibits *in vitro* transcription and topoisomerase I
258 activity, Lsr2 localizes near the replisome, and alters *M. smegmatis* progression through the cell
259 cycle (42, 48, 49). Thus, we hypothesized that Lsr2 affects the dynamics or localization of
260 DnaE1, a key mediator of replisome function and DNA replication fidelity.

261

262 **Lsr2 alters replisome dynamics throughout the cell cycle**

263 To investigate the dynamics of DnaE1, we visualized DnaE1-mScarletI in wild type and
264 Δ*lsr2* cells by expressing this fusion from the native promoter. A similar fusion encodes
265 functional DnaE1 (56). We next performed time-lapse microscopy and analyzed fluorescence
266 distributions as a function of both cell length and cell cycle. Consistent with the reported
267 placement of the replisome in mycobacteria, DnaE1 localizes at approximately mid cell, before
268 disappearing presumably after DNA replication has been completed (56). Towards the end of
269 the cell cycle, DnaE1 reappears at one- and three-quarter positions to initiate replication in
270 newly synthesized sister chromosomes. Consistent with prior findings using a DnaN reporter,
271 DNA replication is faster in cells missing *lsr2*, lasting for roughly one-half of the cell cycle (~70
272 minutes) versus approximately two-thirds of the cell cycle (~100 minutes) in wild type (**Fig 5A**)
273 (48). In our conditions, cells divide on average every 150 minutes, as defined by the time
274 between successive septal invagination events visualized by phase contrast microscopy.

275 We reasoned that Lsr2 could be affecting replisome dynamics directly or indirectly. To
276 address this, we constructed a strain harboring fluorescent translational fusions to Lsr2 and
277 DnaE1. ChIP-seq data show an abundance of Lsr2 binding sites across the chromosome;
278 consistent with this, we find that Lsr2 decorates the entire nucleoid in discrete and highly
279 dynamic puncta (43). Images at a single time point were ambiguous in relation to the amount of

280 co-localization between DnaE1 and Lsr2 (**Fig 5B**). Thus, we performed time-lapse microscopy
281 and, as before, constructed kymographs to visualize the probability distribution of Lsr2's
282 localization in both space and time. We find that Lsr2 is enriched near the pole of the cell and
283 that localization tracks with cell elongation (**Fig 5C**). Consistent with prior findings, Lsr2 localizes
284 nearby DnaE1 at certain times in the cell cycle, but does not co-localize with it, despite Lsr2's
285 abundance throughout nucleoid. Taken together, our data suggest that Lsr2 may be excluded
286 from the replisome, and in its absence, DNA replicates more quickly in standard laboratory
287 growth media (48). Thus, Lsr2 may be acting as an obstacle for DNA replication.

288

289 **Lsr2 promotes frequent exchange of the polymerases in the replisome**

290 In *E.coli*, replisome components exchange rapidly, likely when encountering DNA-
291 protein obstacles. That is, FRAP and single molecule studies have revealed that, despite being
292 highly processive *in vitro*, replisome components are highly dynamic within the cell (57). For
293 example, at room temperature, the alpha subunit of Pol III in *E. coli* exchanges with the
294 cytoplasmic pool at a time scale of approximately 4 seconds, suggesting that subunits are
295 constantly being replaced during the 150 minutes it takes to replicate the chromosome at this
296 temperature (57). These data underlie the notion that the replisome is dynamic and flexible,
297 allowing new subunits and components the opportunity to exchange frequently.

298 We reasoned that if Lsr2 prevented fast replication of the chromosome, then it might
299 also affect the timescale of polymerase exchange. To test this, we took the same approach as
300 Beattie, TR *et al* and used FRAP to measure the dynamics of recovery of DnaE1 in cells with or
301 without Lsr2 (57). Fast recovery of fluorophores into a bleached spot indicates fast dissociation
302 of bleached molecules. Conversely, slow, or incomplete recovery of non-bleached fluorophores
303 indicates slow dissociation of bleached molecules, and a stably associated complex. To account

304 for differences in the degree of bleaching per cell, we normalized the fluorescence intensity after
305 bleaching to zero, and the final intensity to the maximum recovery we expected based on the
306 percentage of fluorophores bleached. We fit the data to a diffusion exchange reaction and
307 calculated both the timescale of recovery, reflecting the dissociation time of bound subunits, and
308 the maximum recovery, reflecting the mobile fraction of proteins. Imaging was done in the same
309 conditions as above, in which we measure the duration of chromosomal replication to be
310 approximately 100 minutes. DnaE1 had dramatically different timescales of exchange in wild
311 type and mutant cells. In wild type cells, consistent with similar measurements done in *E.coli*,
312 DnaE1 exchanged quickly and nearly completely with a timescale of approximately 8.09 +/- 3.11
313 seconds (mean±SD). In contrast, DnaE1 recovery occurred at a much longer timescale in *Δlsr2*
314 cells, exchanging with a timescale of 38.10 +/- 9.96 seconds (**Fig 5D, 5E, 5F**). As DnaE1 is a
315 highly faithful and processive enzyme, these data are consistent with faster replication time and
316 lower mutation rate of the *lsr2* mutant in these conditions (9).

317 We next wondered if Lsr2 also affected polymerase exchange in conditions that elevate
318 expression of the error-prone polymerase DnaE2 and its associated complex. To test this, we
319 created constructs that translationally fused ImuA', ImuB, and DnaE2 to fluorescent proteins.
320 ImuA' and ImuB fusions restored elevated mutation frequency in Δ*imuA'B* cells, as did a
321 chromosomal DnaE2-GFPmut (**Fig S5A, S5B**)(34). Notably, others have reported that ImuA'
322 and ImuB fluorescent fusions do not complement a small growth defect of Δ*imuA'B* on MMC-
323 containing agar (34). Based on their ability to restore mutation, we concluded that ImuA', ImuB,
324 and DnaE2 fusions were at least partly, if not entirely, functional.

325 Despite being co-transcribed, ImuA' and ImuB had dramatically different fluorescent
326 intensities: ImuB was brightly fluorescent, while ImuA' was barely detectable above the
327 background (**Fig S6A, S6B**). Thus, cellular levels of ImuA' are much lower than ImuB, implying
328 that additional post-transcriptional mechanisms exist (e.g. translation regulation or proteolysis)

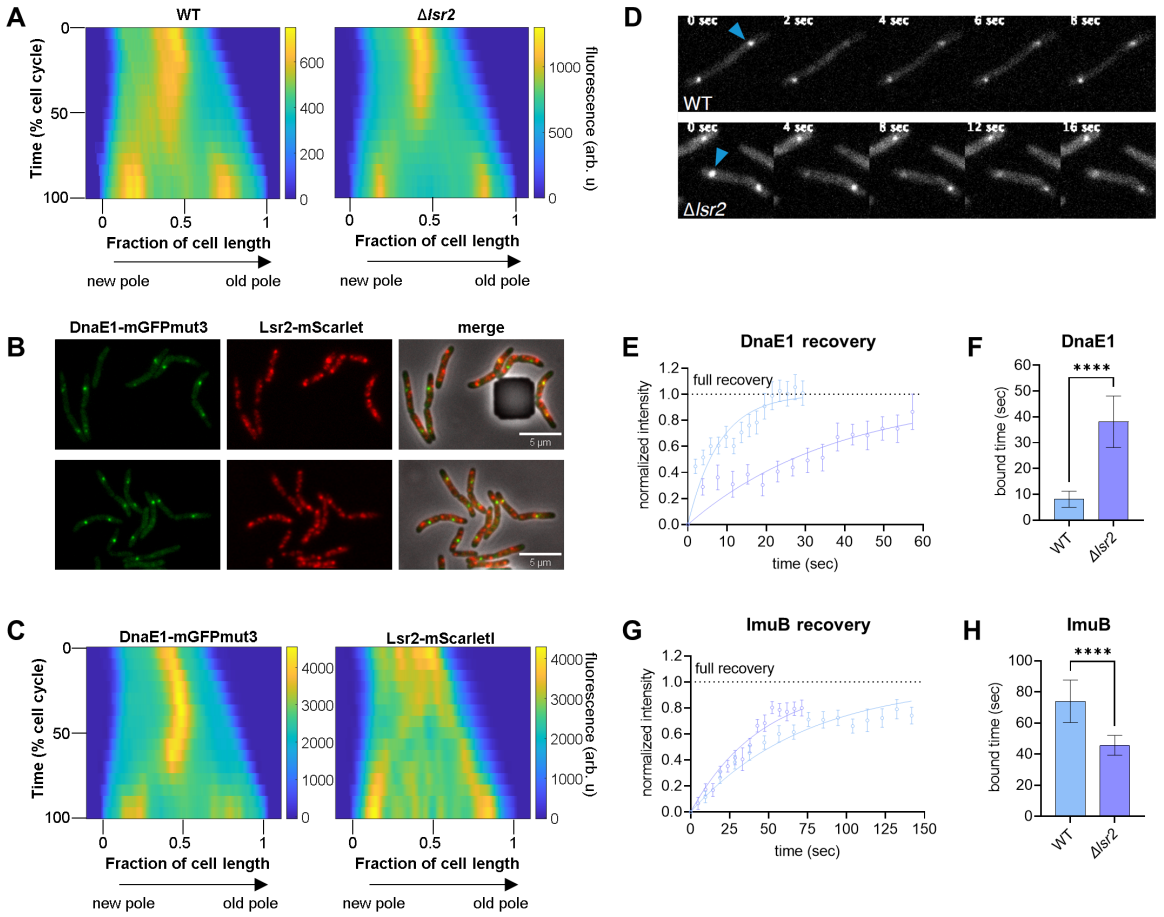

FIGURE 5. Loss of *lsr2* changes replicative polymerase and translesion complex dynamics. (A) Kymograph of DnaE1-mScarlet expressed from the native promoter on a phage integrative plasmid in WT (left) or Δ*lsr2* (right). (**B, C**) Microscopy images and kymograph of cells expressing DnaE1-mGFPmut3 and Lsr2-mScarlet in a Δ*lsr2* background. **(D)** FRAP of DnaE1-mScarlet in WT (top) and Δ*lsr2* (bottom) imaged at 2 and 4 second intervals, respectively. Blue arrow indicates the location of the focus targeted for bleaching. **(E)** and **(G)** show the fluorescence recovery curves for DnaE1-mScarlet (N=21 for WT, 12 for Δ*lsr2*) and mScarlet-ImuB (N=13 for WT, 10 for Δ*lsr2*). Solid lines show a one-phase exponential association fit to the data. Individual points show the mean±SEM of fluorescence intensity after bleach correction. Dashed line represents the estimated maximum possible fluorescence recovery. **(F)** and **(H)** show bound times (mean±SD) obtained from one-phase exponential association fits for DnaE1 and ImuB, respectively.(**G, H**) DNA damage was induced by treatment with mitomycin C (1.56 ng/ml) for 4 hours. p-values were obtained by unpaired t-test. For all panels: 0.1234 (ns), 0.0332 (*), 0.0021 (**), 0.0002 (***), <0.0001 (****).

329 to limit ImuA' abundance. Like ImuA', DnaE2 was also very dim (**Fig S6C**). These data suggest

330 that one limiting factor in forming an active mutasome complex may be the low cellular

331 concentrations of ImuA' and/or DnaE2. Due to the low abundance of ImuA' and DnaE2 it was

332 difficult to draw conclusions about their localization or dynamics in cells with or without *lsr2*.
333 Thus, we decided to determine the exchange rate of ImuB, which recruits ImuA' and DnaE2 into
334 an active complex by binding to the β-clamp subunit of the replisome, and thus is a key factor in
335 the stability of the mutasome. To test the recovery of ImuB, we treated cells with a low
336 concentration of mitomycin to induce its expression and again performed FRAP. ImuB displayed
337 a much longer timescale of exchange than DnaE1 (73.97 +/- 13.65 seconds), suggesting the
338 protein remains associated with the β-clamp for a long time (**Fig 5G, 5H**). Such a long-bound
339 time may be necessary to recruit the lowly abundant proteins ImuA' and DnaE2. In cells missing
340 *lsr2*, ImuB exchanged more quickly (45.66 +/- 6.36 seconds), suggesting that the mutasome
341 complex is less stably associated in these cells.

342 These data lead to a model whereby in non-DNA damaging conditions, Lsr2 serves as
343 an obstacle that promotes the frequent exchange of DnaE1, thus preventing collisions with
344 transcription factors, and allowing other polymerases to exchange into the replisome (**Fig 6**).
345 This model is consistent with *Δlsr2* having a slightly reduced basal mutation rate, as Lsr2 could
346 be allowing exchange of polymerases besides DnaE1 at a low frequency. Likewise, in DNA
347 damaging conditions, Lsr2-mediated exchange of DnaE1 promotes loading of ImuB and thus
348 DnaE2 and ImuA'. DnaE1 is a more faithful enzyme but is unable to bypass lesions; thus, cells
349 missing *lsr2* grow more slowly under conditions that damage DNA but replicate with higher
350 fidelity.

351

352 **DISCUSSION**

353 Lsr2 acts as a transcriptional repressor for many genes on the *M. smegmatis* and *M.*
354 *tuberculosis* chromosomes (41, 42, 43, 44). Additionally, multiple lines of evidence suggest that
355 *lsr2* has other roles aside from its function as a transcription factor (41, 48, 49). Our results

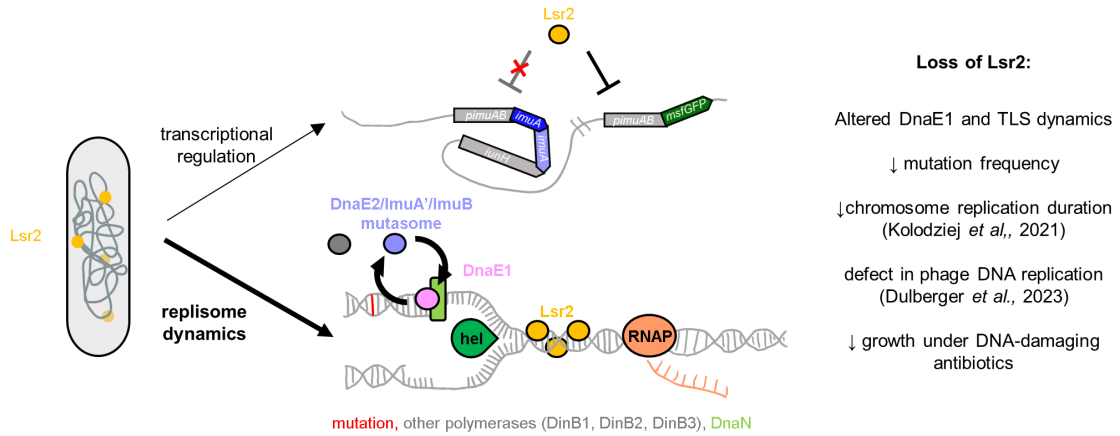

FIGURE 6. Model of Lsr2 regulation of DNA replication and mutagenesis. Lsr2 transcription factor activity is only partly determined by sequence, as the same sequence in different genomic contexts can be regulated by Lsr2 or not. Instead, our data suggest that loss of *lsr2* results in a decrease in mutagenesis due to a novel role for Lsr2 in modulating replisome dynamics. Specifically, our data are consistent with a model in which Lsr2 acts as a roadblock on the DNA to promote the exchange of the major replicative polymerase DnaE1 with others in the cytoplasmic pool. In conditions that do not induce DNA damage, these polymerases likely include DinB1, which is responsible, in part, for spontaneous mutation. In conditions that damage DNA, the mutasome, which is comprised of DnaE2 and its accessory proteins, ImuA' and ImuB, are induced and need to exchange with the replicative polymerase to repair lesions. Deletion of *lsr2* reduces the flexibility of the replisome needed for sufficient exchange, thereby resulting in cells that are more reliant on DnaE1, a high fidelity polymerase that unable to bypass lesions. Thus, cells missing *lsr2* are impaired in their ability to grow in conditions that damage DNA in their ability to acquire mutations.

356 advance our understanding of both functions of Lsr2, and implicate Lsr2 as a potential factor in
357 the emergence of mycobacterial antibiotic resistance.

358 Lsr2 can control transcription directly by binding promoter regions or indirectly, such as
359 by altering DNA structure (43). Consistent with studies of *Streptomyces* Lsr2 and of the *E.coli* H-
360 NS, prior studies identified no consensus motifs for Lsr2 binding in mycobacteria and
361 demonstrated increased Lsr2 binding in AT-rich sequences (42, 45, 58, 59). Our study identifies
362 the sequence context as an additional factor in Lsr2 regulation. We find that the sequence
363 context may permit or prohibit Lsr2 regulation, resulting in a discrepancy between promoter-
364 reporter constructs and endogenous RNA levels for some genes. While we do not yet know if
365 Lsr2 regulation is direct or indirect, it is possible that changes in the DNA structure may affect

366 Lsr2 access to the DNA. Lsr2 access to the DNA may also be mediated by other proteins,
367 including other NAPs and transcription factors. Further experiments are necessary to define the
368 mechanism by which the sequence context mediates Lsr2 regulation.

369 While Lsr2 binds to and/or alters the transcription of many genes in both *M. smegmatis*
370 and *M. tuberculosis,* very few phenotypes associated with the deletion mutant have been
371 connected to altered expression of target genes (41, 42, 43). One of the few exceptions is the
372 change in colony morphology, which can be attributed to the increased expression of a putative
373 polyketide synthase (MSMEG_4727) in *M. smegmatis* (43, 60). Why then is Lsr2 associated
374 with so many bacterial behaviors including bacterial growth, the cell cycle, robust infection,
375 survival to hydrogen peroxide and antibiotics, survival in low oxygen, and resistance to phage?

376 Our results indicate that one of Lsr2's main functions in the cell is to promote the
377 flexibility of the mycobacterial replisome, enabling specialist polymerases like the DnaE2
378 translesion complex (ImuB/DnaE2/ImuA') to access the replication fork, leading to efficient, but
379 error-prone, DNA replication and cell growth in conditions that damage DNA. Numerous studies
380 in eukaryotes and other bacteria show that the rate of replication fork progression is actively
381 regulated, in some cases by machinery that slow down DNA replication, to ensure coordination
382 amongst DNA replication, DNA repair, and transcription (61, 62, 63, 64). We hypothesize that
383 Lsr2 may function to regulate replication fork progression in mycobacteria, and that this function
384 may provide a unifying explanation for many of the phenotypes associated with loss of *lsr2,*
385 including slower DNA replication in the host and other environmental conditions likely to assault
386 DNA. Likewise, in conditions that do not significantly damage DNA, like those found in
387 laboratory growth media, loss of *lsr2* leads to faster and higher fidelity chromosomal replication,
388 possibly explaining the emergence of spontaneous *lsr2* mutants in several laboratories including
389 our own (60, 65, 66). Additionally, loss of *lsr2* is associated increased resistance against
390 infection by certain phages, and fewer and smaller zones of phage DNA replication (49). We

391 speculate that efficient turnover of the bacterial host DNA replication machinery mediated by
392 Lsr2 could be required for robust replication of phage DNA and productive infection.

393 Intriguingly, Lsr2 is phosphorylated by PknB, a plasma membrane-bound eukaryotic
394 serine/threonine kinase involved in cell growth and division (67). Future research is needed but
395 we speculate that such regulation could be used to coordinate cell wall synthesis and DNA
396 synthesis during environmental changes or even during the course of a typical cell cycle.

397 Lsr2 may be a promising drug target for preventing the emergence of antibiotic
398 resistance in mycobacteria. Our work adds to the growing body of evidence Lsr2 is at the nexus
399 of several evolutionary tradeoffs, including fast chromosome replication, mutagenesis,
400 replisome flexibility, and phage resistance. Indeed, loss of Lsr2 results in severe growth defects
401 in *M. tuberculosis* and *M. abscessus in vivo* (44, 46). Thus, we speculate that targeting Lsr2
402 therapeutically may help treat drug-susceptible infections, while preventing the emergence of
403 drug resistance.

404

405

406 **RESOURCE AVAILABILITY**

407 **Lead contact**

408 Further information and requests for resources and reagents should be directed to and will be
409 fulfilled by the lead contact, Dr. Hesper Rego (hesper.rego@yale.edu).

410

411 **Materials availability**

412 All unique/stable reagents generated in this study are available from the lead contact.

413

414 **MATERIALS AND METHODS**

415 **Strains and growth conditions**

416 All mycobacterial strains are derivatives of *Mycobacterium smegmatis* MC2 155. Cells were
417 grown in Middlebrook 7H9 broth supplemented with 0.05% (v/v) Tween80, ADC, and 0.2% (v/v)
418 glycerol for liquid culture. LB agar was used as solid media. Liquid cultures were grown at 37 °C
419 on a rotator. Agar plates were incubated at 37 °C. If applicable, antibiotics were added at the
420 following final concentrations: hygromycin B (50 ug/mL), kanamycin (25ug/mL), nourseothricin
421 (20 ug/ml), zeocin (20 ug/mL), and gentamicin (5 ug/ml).

422 Plasmid DNA for transformation into *M. smegmatis* was prepared from E.coli (DH5a,
423 XL1). If applicable, antibiotics were added at the following final concentrations: hygromycin B
424 (100 ug/mL), kanamycin (50 ug/mL), and nourseothricin (40 ug/ml). Plasmid constructs were
425 generated using Gibson cloning and phage-based integrative vectors. Fluorescent promoter
426 reporters were made by fusing a 500 bp region upstream the start codon of the target gene
427 (e.g., *imuA'B*, *dnaE2*) to the native start codon and fluorescent protein (e.g., *msfGFP*, *mScarletI*)

428 coding sequence. *imuA'B* expression constructs were made using a similar approach as the
429 fluorescent reporter constructs, but using the *imuA'B* coding sequence. For *msfGFP* and *imuA'B*
430 constructs denoted (+)DS, the 1.55kb sequence downstream the endogenous *imuB* was cloned
431 downstream the *msfGFP* or *imuB* coding sequence in the phage integrative construct,
432 respectively.

433 Genetic modifications to the native locus were generated as previously described using
434 the mycobacterial Che9c phage RecET recombination system (40). To construct a knockout, we
435 designed a dsDNA substrate encoding a zeocin resistance cassette flanked by loxP sites and
436 ~500bp of homology on either end of the locus of interest. The dsDNA substrate was then
437 electroporated into *M. smegmatis* strains carrying a plasmid encoding isovaleronitrile-inducible
438 expression of RecET. Colonies were selected by zeocin resistance and screened by PCR using
439 primers annealing to regions flanking dsDNA insertion. In some cases, the zeocin resistance
440 cassette was removed by Cre-Lox recombination. Primers and strains are listed in Table S1 and
441 S2. mc^2155 Δ*pafBC* is a gift of the Weber-Ban lab, and was generated using the *rpsL*
442 counterselection strategy (39).
443

444 **Flow cytometry**

445 Flow cytometry was performed on fixed cells with doublet discrimination. To induce DNA
446 damage, cells were treated with mitomycin C (80 ng/ml) for 9 hours unless otherwise noted.
447 Cells were fixed 1% paraformaldehyde in PBS+0.05% Tween-80 (PBST) for 10 minutes, and
448 washed twice and resuspended in PBST prior to flow cytometry. Flow cytometry data were
449 analyzed using FlowJo software.
450

451 **Fluorescence microscopy**

452 All microscopy experiments were performed on a Nikon TI-E inverted wide-field microscope
453 equipped with the Nikon Perfect Focus System, an ORCA-Flash4.0 Digital CMOS Camera
454 (Hamamatsu) and an environmental control chamber maintained at 37 °C.
455
456 **Time-lapse and kymograph analysis:** Time-lapse imaging was done using a 60X Oil 1.45NA
457 Plan Apochromat phase-contrast objective. Bacterial samples were loaded and grown in a B04A
458 microfluidic plate (CellAsic ONIX, B04A-03-5PK). Phase and fluorescence images were
459 acquired every 30 minutes using NIS Elements software. Fluorescence images were taken
460 sequentially using a 470 nm excitation laser and 515/30 emission filter for msfGFP and
461 mGFPmut3, and a 555 nm excitation laser and a 595/40 emission filter for mScarletI.
462 Kymograph analysis was performed using a custom pipeline for segmenting and tracking
463 cells, and extracting fluorescence profiles. Cell segmentation was performed on the phase
464 image using a U-Net network trained for segmenting mycobacterial cells (68). Semi-automated
465 cell tracking and extraction of fluorescence profiles from background-subtracted images was
466 done using a custom MATLAB program and open-source image analysis software Fiji (69).
467 Average kymographs were generated by 2D interpolation of at least twenty individual
468 kymographs.
469
470 **FRAP:** FRAP experiments were done using a 60X oil DIC objective. Bacterial cells were imaged
471 under 7H9 agar pads (1% agar, 0.2% (v/v) glycerol) in 50 mm glass-bottomed dishes.
472 Fluorescent spots were manually selected for localized bleaching with a focused 405-nm laser.
473 Two pre-bleach fluorescence images were acquired: one to identify and center a target focus,
474 and a second for quantification of total pre-bleach fluorescence. Fluorescence recovery was
475 monitored by acquisition at pre-defined intervals (2 to 10 sec) following photobleaching using an
476 exposure time of 200 ms.

477 Cell outlines for determination of total pre-bleach fluorescence were manually drawn
478 using the brightfield image. Fluorescence images were background subtracted and corrected for
479 photobleaching. To quantify the fluorescence of bleached foci over time, a circular ROI was
480 manually drawn around the bleached foci and intensity profiles over time were obtained using
481 Fiji (69). Fluorescence recovery curves were generated by first normalizing fluorescence
482 intensity profiles to pre-bleach focus fluorescence. The post-bleach value was then subtracted
483 from all time points. Maximum recovery was estimated by calculating the total amount of
484 fluorescence in the cell after photobleaching outside the focus. Finally, all time points were
485 divided by the estimated maximum recovery value, such that a value of 0 and 1 correspond to
486 no recovery and maximum recovery, respectively.
487
488 **RNA-seq of WT *M. smegmatis* and Δ*lsr2***
489 WT *M. smegmatis* and Δ*lsr2* were grown in triplicate at 37°C to OD600 ~0.7-1.0. For mitomycin
490 treatment, 1 ml of cells were added to 4 ml of 7H9 containing 100 ng/ml mitomycin C for a final
491 concentration of 80 ng/ml mitomycin C. Approximately 2-4 ml of cells were harvested at each
492 timepoint and incubated with 2 volumes of RNAprotect (Qiagen) at room temperature for 5
493 minutes prior to centrifugation for 5 minutes at 4000xg 4°C. The supernatant was discarded,
494 and the cells were then immediately used for RNA extraction or stored at -80°C.
495 RNA extraction was performed using the Qiagen RNeasy Kit (74104). Cells were
496 resuspended in 500 ul of RLT buffer (Qiagen) with 2-mercaptoethanol and homogenized by
497 bead beating for 3 minute pulses at maximum speed, three times, with 5 minutes of rest on ice
498 in-between. The lysate was then centrifuged at maximum speed for 1 minute, and the
499 supernatant was transferred to a new tube. The remainder of the RNA extraction was performed
500 using the Qiagen RNeasy Kit according to manufacturer instructions. RNA quality was verified
501 using a bioanalyzer (Agilent Technologies TapeStation 2200). DNase treatment and ribosomal

502 RNA depletion were performed at the Microbial Genome Sequencing Center before library
503 preparation and sequencing.
504
505 **RT-qPCR**
506 RNA was extracted as described for RNA-seq studies. RNA was DNAse-treated for 30 minutes
507 at 37 °C twice, and then cleaned using the Zymo RNA Clean and Concentrator kit. cDNA
508 synthesis and qPCR was performed using SuperScript IV First-strand Synthesis System & iTaq
509 Universal SYBR Green Supermix, respectively. RNA levels were normalized to *sigA.* All
510 experiments were done in triplicate. RT-qPCR primers are listed in **Table S1**.
511
512 **Mutation frequency analysis**
513 10 ml of bacterial cells were grown to OD600 ~0.7-1.0. 5 ml of cells were UV irradiated (20
514 mJ/cm2 UV; Stratalinker UV crosslinker), while the remaining 5 ml of cells were used for the
515 untreated control. Treated and untreated samples were then added to an equal volume of fresh
516 7H9 media and outgrown for 3 hours at 37°C. 100 ul liquid culture was used for CFU
517 determination, and the remainder of the culture was plated onto Rif-containing LB agar plates
518 (200 ug/ml) for mutant detection. All mutation frequency measurements were performed using 8
519 biological replicates. Rif-resistant colonies were enumerated after 5-7 days of incubation at
520 37°C. CFU plates were read after about 2-3 days of growth on non-selective media. Mutation
521 frequencies were calculated by the number of Rif-resistant colonies per ml of culture by the
522 CFU/ml.
523
524 **Spot assay**
525 Bacterial cells were grown to OD600 ~0.7-1.0, normalized to the same OD, and then 10-fold
526 serially diluted. 5 ul of culture were spotted on LB agar containing varying concentrations of

527 antibiotic. Plates were imaged after incubation at 37°C for 2-3 days. All assays were done in
528 biological triplicate.

529

530 **Tn-seq**

531 Transposon libraries in wild type and Δ*lsr2* were prepared as and sequenced described
532 elsewhere (70). The TRANSIT and TPP python packages were used to map insertions to the
533 mc^2155 genome and quantitatively compare insertions across stains, using the 'resampling'
534 option (71).

535

536 **ACKNOWLEDGMENTS**

537 mc2155 SMR5 Δ*pafBC* was generously provided by Dr. Elika Weber-Ban. We thank members
538 of the Rego lab for helpful suggestions, and Dr. Eduardo Groisman for discussions. We also
539 thank the Yale Flow Cytometry Facility for technical assistance with flow cytometry experiments.
540 This work was supported by the Searle and Pew Foundations to EHR.

541

542 **AUTHOR CONTRIBUTIONS**

543 WLN and EHR conceived experiments. JHP performed Tn-seq and Tn-seq analysis; WLN
544 performed other experiments and analyzed data. WLN and EHR wrote the manuscript. EHR
545 secured funding for the work.

546

547

548

549 **SUPPLEMENTARY INFORMATION**

550
551
552
553

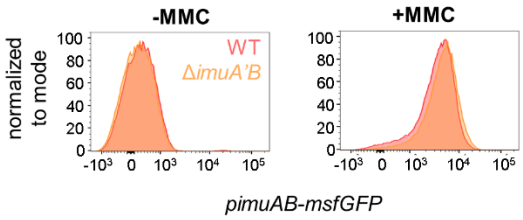

554
555
556
557
558 **FIGURE S1. *imuA'B* deletion does not affect *pimuAB* reporter levels.** Flow cytometry

559 histograms of strains harboring *pimuAB* reporter at the Giles *attB* site in either a wild-type (red)

560 or Δ*imuA'B (*orange) background for one biological replicate. DNA damage was induced by

561 mitomycin C treatment (80 ng/ml, 9 hours).

562

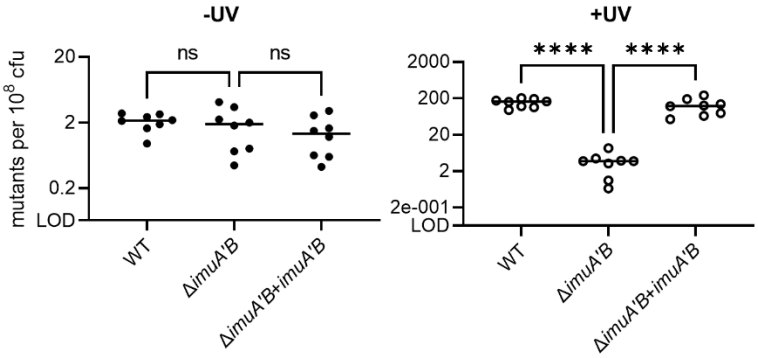

563

564 **FIGURE S2. *imuA'B* is required for UV-induced mutagenesis. *ΔimuA'B* exhibits frequency**

565 **of UV-induced mutants** Frequency of rifampin-resistant mutants per 10^8 cfu without (left) or

566 with (right) UV-induced DNA damage (20 mJ/cm^2 UV). Strains are WT, Δ*imuA'B*, and Δ*imuA'B*

567 complemented with *imuA'B* expressed from the native *imuA'B* promoter on a phage integrative

568 plasmid. LOD refers to the limit of detection. p-values were obtained by one-way ANOVA.

569 0.1234 (ns), 0.0332 (*), 0.0021 (**), 0.0002 (***), <0.0001 (****).

570

571

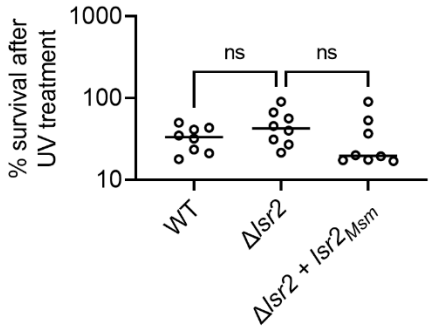

572

573 **FIGURE S3. WT and Δ*lsr2* survival after UV treatment.** Loss of *lsr2* is not associated with a

574 decrease in survival following UV treatment (20 mJ/cm^2). Strains are WT, Δ*lsr2*, and Δ*lsr2*

575 complemented with *lsr2* expressed from the native *lsr2* promoter on a phage integrative

576 plasmid. Percent survival is the ratio of cfu/ml for UV-treated cells divided by the cfu/ml for

577 untreated cells multiplied by 100. p-values were obtained by one-way ANOVA. 0.1234 (ns),

578 0.0332 (*), 0.0021 (**), 0.0002 (***), <0.0001 (****).

579

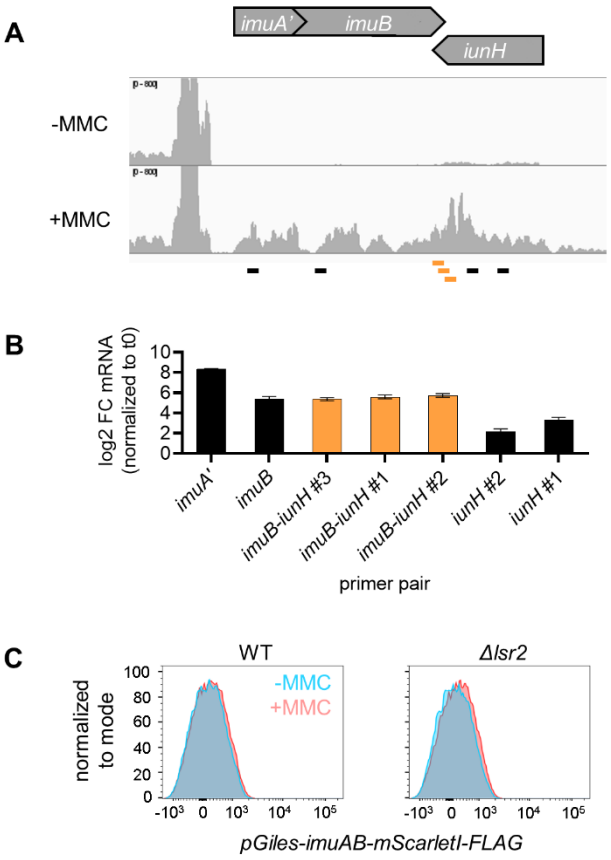

580

581 **FIGURE S4. Antisense *iunH* reads most likely originate from transcriptional readthrough**
582 **of *imuA'B*. (A)** Schematic of *imuA'B-iunH* locus and IGV visualization of RNA-seq reads in the
583 absence (top) and presence (bottom) of mitomycin C (80 ng/ml, 24 hours). **(B)** Log2 fold-change
584 in mRNA levels in mitomycin C-treated samples (80 ng/ml, 9 hours) relative to levels in
585 untreated samples for the following amplicons, in order from left to right: *imuA'* coding
586 sequence, the *imuB* coding sequence, three different amplicons spanning the *imuB-iunH*
587 junction, and two amplicons for the *iunH* coding sequence. Amplicons are represented by black
588 and orange lines across the bottom of **(A)**. Orange lines and bars in **(A)** and **(B)** correspond to
589 amplicons that span the junction of the *imuB* and *iunH* coding sequences. **(C)** Flow cytometry
590 histograms of strains harboring the *imuAB* coding sequence transcriptionally fused to the
591 *mScarletI* fluorescent protein at the Giles *attB* site in either a wild-type (left) or Δ*imuA'B (*right)

592 background for one biological replicate. DNA damage was induced by mitomycin C treatment

593 (80 ng/ml, 9 hours).

594

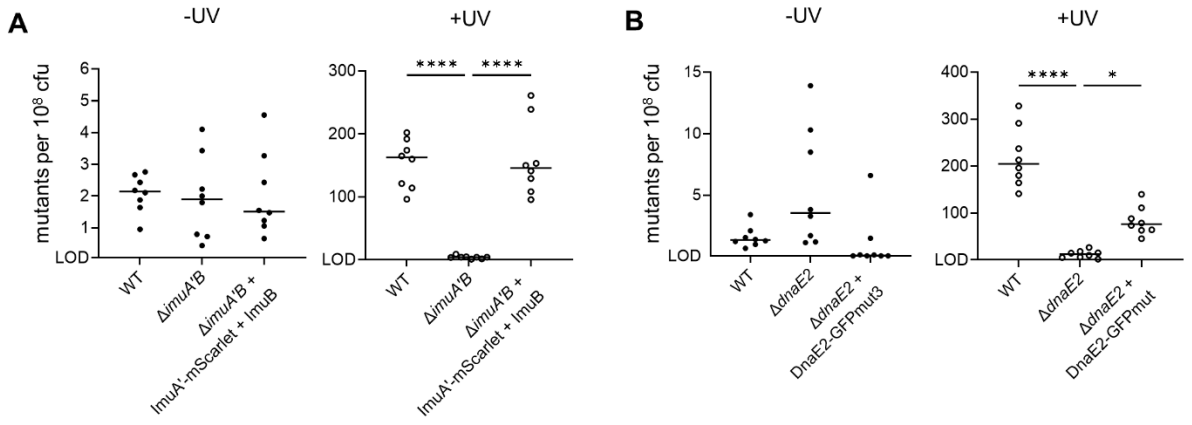

FIGURE S5. ImuA' and DnaE2 translational fusions maintain functionality in UV-induced mutagenesis. Frequency of rifampin-resistant mutants per 10^8 cfu without or with UV-induced DNA damage (20 mJ/cm^2 UV). **(A)** Results shown are for WT, *imuA'B* deletion, or *imuA'B* deletion complemented with a fluorescent translational fusion of ImuA' and ImuB. **(B)** Results shown are for WT, *dnaE2* deletion, and *dnaE2* deletion complemented with a fluorescent translational fusion of DnaE2. Complements are expressed from the native promoter on a phage integrative plasmid. LOD refers to the limit of detection. p-values were obtained by one-way ANOVA. 0.1234 (ns), 0.0332 (*), 0.0021 (**), 0.0002 (***), <0.0001 (****).

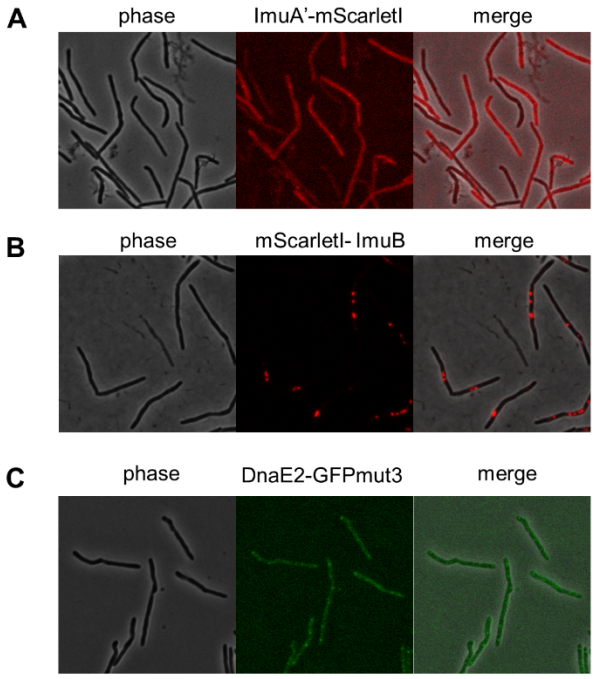

FIGURE S6. Microscopy images of mutasome translational fusions. Images shown are of (A) *imuA'B* deletion mutant complemented with a fluorescent translational fusion of ImuA' and ImuB, **(B)** *imuA'B* deletion mutant complemented with ImuA and a fluorescent translational fusion of ImuB, and **(C)** *dnaE2* deletion mutant complemented with a fluorescent translational fusion of DnaE2. Complements are expressed from the native promoter on a phage integrative plasmid. DNA damage was induced by mitomycin C treatment (80 ng/ml) for 4-6 hours. Images were acquired using 1 second **(A, B)** or 500 ms **(C)** exposure times.

618 **TABLE S1.** Primer list

619 *see attached

620

621 **TABLE S2.** Strain list

STRAIN	GENOTYPE	SOURCE	Additional information
HRCT117	DH5a / pJR962	Gift of the Rock Lab (36)	Backbone for CRISPRi constructs
WN701	mc2155 L5::pJR962ΔTetR-non-targeting sgRNA Tweety::pdnaE2-mScarlet-FLAG Giles::pimuAB-msfGFP-myc	This work	WT *M. smegmatis* with non-targeting CRISPRi construct, and *pdnaE2* and *pimuAB* reporters
WN702	mc2155 L5::pJR962-LexA sgRNA Tweety::pdnaE2-mScarlet-FLAG Giles::pimuAB-msfGFP-myc	This work	WT *M. smegmatis* with *lexA*-tareting CRISPRi construct, and *pdnaE2* and *pimuAB* reporters
WN414	mc2155 SMR5 ΔpafBC	Gift of the Weber-Ban lab (39)	
WN421	mc2155 SMR5 ΔpafBC Tweety::pdna-mScarletI-FLAG Giles::pimuAB-msfGFP-myc	This work	*pafBC* deletion strain with *pimuAB* and *pdnaE2* reporters
WN788	mc2155Δlsr2::zeoR	This work	*lsr2* deletion strain
WN977	mc2155 Giles::pimuab-msfGFP-myc	This work	*pimuAB* reporter in WT background
WN1014	mc2155Δlsr2::zeoR Giles::pimuab-msfGFP-myc	This work	*pimuAB* reporter in Δ*lsr2* background
WN1139	mc2155Δlsr2::zeoR Giles::pimuab-msfGFP-myc Tw::pNative-MSMEG6092	This work	*pimuAB* reporter in Δ*lsr2* background, complemented with untagged *M. smegmatis* Lsr2
WN1342	mc2155Δimuab::msfGFP-myc-loxP	This work	*pimuAB* reporter at native locus in a WT background
WN1348	mc2155Δimuab::msfGFP-myc-loxP Δlsr2::zeoR	This work	*pimuAB* reporter at native locus in a Δ*lsr2* background
WN906	mc2155Δlsr2::zeoR L5::plsr2-mScarletI-FLAG Giles::pimuAB-msfGFP-myc Tweety::pNative-MSMEG6092	This work	*lsr2* deletion strain, complemented with untagged *M. smegmatis* Lsr2
WN874	mc2155Δlsr2::zeoR Giles::pimuAB-msfGFP-myc Tw::pdnaE2-mScarletI-FLAG L5::pNative-Rv3597c	This work	*lsr2* deletion strain, complemented with untagged *M. tuberculosis* Lsr2
WN296	mc2155 Tweety::pdnaE2-500-mScarletI-FLAG Giles::pdnae2-msfGFP-myc	This work	*pdnaE2* reporter in a WT background
WN288	mc2155 Tweety::pdnaE2-mScarletI-FLAG Giles::p2723-msfGFP-myc	This work	*precA* reporter in a WT background
WN287	mc2155 Tweety::pdnaE2-mScarletI-FLAG Giles::plexa-msfGFP-myc	This work	*plexA* reporter in a WT background
WN284	mc2155 Tweety::pdnaE2-mScarletI-FLAG Giles::p2742-msfGFP-myc	This work	*pchiZ* reporter in a WT background
WN285	mc2155 Tweety::pdnaE2-mScarletI-FLAG Giles::p5451-msfGFP-myc	This work	*p5451* reporter in a WT background
WN291	mc2155 Tweety::pdnaE2-mScarletI-FLAG Giles::p6573-msfGFP-myc	This work	*p6573* reporter in a WT background
WN286	mc2155 Tweety::pdnaE2-mScarletI-FLAG Giles::p6837-msfGFP-myc	This work	*p6837* reporter in a WT background
WN845	mc2155Δlsr2::zeoR Giles::pdnae2-msfGFP-myc	This work	*pdnaE2* reporter in a Δ*lsr2* background
WN834	mc2155Δlsr2::zeoR Giles::p2723-msfGFP-myc	This work	*precA* reporter in a Δ*lsr2* background

WN843	mc2155Δlsr2::zeoR Giles::plexa-msfGFP-myc	This work	*plexA* reporter in a Δ*lsr2* background
WN835	mc2155Δlsr2::zeoR Giles::p2742-msfGFP-myc	This work	*pchiZ* reporter in a Δ*lsr2* background
WN841	mc2155Δlsr2::zeoR Giles::p5451-msfGFP-myc	This work	*p5451* reporter in a Δ*lsr2* background
WN839	mc2155Δlsr2::zeoR Giles::p6573-msfGFP-myc	This work	*p6573* reporter in a Δ*lsr2* background
WN842	mc2155Δlsr2::zeoR Giles::p6837-msfGFP-myc	This work	*p6837* reporter in a Δ*lsr2* background
WN1140	mc2155 L5::pJR962-LexA sgRNA Giles::pimuAB-msfGFP-myc	This work	*msfGFP* expression construct without downstream sequence in WT
WN1141	mc2155Δlsr2::zeoR L5::pJR962-LexA sgRNA Giles::pimuAB-msfGFP-myc	This work	*msfGFP* expression without downstream sequence in Δ*lsr2*
WN1158	mc2155 L5::pJR962-LexA sgRNA Giles::pimuAB-500US-msfGFPmyc-1550DS	This work	*msfGFP* expression construct with downstream sequence in WT
WN1160	mc2155Δlsr2::zeoR L5::pJR962-LexA sgRNA Giles::pimuAB-msfGFPmyc-1550DS	This work	*msfGFP* expression with downstream sequence in Δ*lsr2*
WN1166	mc2155ΔimuAB::loxP L5::pJR962-LexA sgRNA Giles::pNative-imuAB	This work	*imuA'B* expression construct without downstream sequence in WT
WN1169	mc2155Δimuab::loxP Δlsr2::zeoR L5::pJR962-LexA sgRNA Giles::pNative-imuAB	This work	*imuA'B* expression without downstream sequence in Δ*lsr2*
WN1167	mc2155ΔimuAB::loxP L5::pJR962-LexA sgRNA Giles::pNative-imuAB-1550DS	This work	*imuA'B* expression construct with downstream sequence in WT
WN1170	mc2155Δimuab::loxP Δlsr2::zeoR L5::pJR962-LexA sgRNA Giles::pNative-imuAB-1550DS	This work	*imuA'B* expression with downstream sequence in Δ*lsr2*
WN1384	mc2155 Giles::pNative-dnae1-mScarletI-FLAG	This work	C-terminal DnaE1 fusion in a WT background; used for kymograph analysis and FRAP
WN1385	mc2155Δlsr2::zeoR Giles::pNative-dnae1-mScarletI-FLAG	This work	C-terminal DnaE1 fusion in a Δ*lsr2* background; used for kymograph analysis and FRAP
WN1390	mc2155Δlsr2::zeoR L5::pNative-MSMEG6092-mScarletI-FLAG Giles::pTetO-DnaE1-mGFPmut3-myc	This work	Dual-labeled C-terminal Lsr2 and C-terminal DnaE1 fusions in a Δ*lsr2* background; used for kymograph analysis
WN1278	mc2155ΔimuAB::loxP L5::pJR962-LexA sgRNA Giles::pNative-imuA_FLAG-mScarletI-imuB-1550DS	This work	N-terminal ImuB fusion in a WT background; used for FRAP
WN1280	mc2155Δimuab::loxP Δlsr2::zeoR L5::pJR962-LexA sgRNA Giles::pNative-imuA_FLAG-mScarletI-imuB-1550DS	This work	N-terminal ImuB fusion in a Δ*lsr2* background; used for FRAP
WN1236	mc2155ΔimuAB::loxP L5::pJR962-LexA sgRNA Giles::pimuAB-msfGFP-myc	This work	*pimuAB* reporter in Δ*imuA'B* background
WN1327	mc2155 Giles::imuAB-mScarletI-FLAG	This work	Fused *imuA'B* coding sequence to mScarletI; WT background
WN1328	mc2155Δlsr2::zeoR Giles::imuAB-mScarletI-FLAG	This work	Fused *imuA'B* coding sequence to mScarletI; Δ*lsr2* background

WN1318	mc2155Δimuab::loxP L5::pJR962-LexA sgRNA Giles::pNative-imuA-mScarletI-FLAG_imuB-1550DS	This work	Translational fusion of ImuA'
WN171	mc2155 rpoB::mApple-hygR dnaE2:: gfpmut3-zeoR	This work	Translational fusion of DnaE2

622

623

624 **TABLES S3 and S4:** *see attached

625 **TABLE S3.** RNA-Seq of *M. smegmatis* wild-type under mitomycin C stress

626 **TABLE S4.** RNA-Seq of *M. smegmatis* Δ*lsr2* under mitomycin C stress

627

628

629 **REFERENCES**

630 1. Fuchs RP, Fujii S. Translesion DNA synthesis and mutagenesis in prokaryotes. Cold
631 Spring Harb Perspect Biol. 2013;5(12):a012682.

632 2. Galagan JE. Genomic insights into tuberculosis. Nature Reviews Genetics.
633 2014;15(5):307-20.

634 3. Boritsch EC, Khanna V, Pawlik A, Honoré N, Navas VH, Ma L, et al. Key experimental
635 evidence of chromosomal DNA transfer among selected tuberculosis-causing mycobacteria.
636 Proceedings of the National Academy of Sciences. 2016;113(35):9876-81.

637 4. Sun G, Luo T, Yang C, Dong X, Li J, Zhu Y, et al. Dynamic population changes in
638 Mycobacterium tuberculosis during acquisition and fixation of drug resistance in patients. J
639 Infect Dis. 2012;206(11):1724-33.

640 5. Mariam SH, Werngren J, Aronsson J, Hoffner S, Andersson DI. Dynamics of antibiotic
641 resistant Mycobacterium tuberculosis during long-term infection and antibiotic treatment. PLoS
642 One. 2011;6(6):e21147.

643 6. Ford CB, Shah RR, Maeda MK, Gagneux S, Murray MB, Cohen T, et al. Mycobacterium
644 tuberculosis mutation rate estimates from different lineages predict substantial differences in the
645 emergence of drug-resistant tuberculosis. Nat Genet. 2013;45(7):784-90.

646 7. McGrath M, Gey van Pittius NC, van Helden PD, Warren RM, Warner DF. Mutation rate
647 and the emergence of drug resistance in Mycobacterium tuberculosis. J Antimicrob Chemother.
648 2014;69(2):292-302.

649 8. Liu Q, Wei J, Li Y, Wang M, Su J, Lu Y, et al. Mycobacterium tuberculosis clinical
650 isolates carry mutational signatures of host immune environments. Sci Adv.
651 2020;6(22):eaba4901.

652 9. Rock JM, Lang UF, Chase MR, Ford CB, Gerrick ER, Gawande R, et al. DNA replication
653 fidelity in Mycobacterium tuberculosis is mediated by an ancestral prokaryotic proofreader. Nat
654 Genet. 2015;47(6):677-81.

655 10. Dupuy P, Ghosh S, Adefisayo O, Buglino J, Shuman S, Glickman MS. Distinctive roles
656 of translesion polymerases DinB1 and DnaE2 in diversification of the mycobacterial genome
657 through substitution and frameshift mutagenesis. Nature Communications. 2022;13(1):4493.

658 11. Boshoff HI, Reed MB, Barry CE, 3rd, Mizrahi V. DnaE2 polymerase contributes to in vivo
659 survival and the emergence of drug resistance in Mycobacterium tuberculosis. Cell.
660 2003;113(2):183-93.

12. Dupuy P, Ghosh S, Fay A, Adefisayo O, Gupta R, Shuman S, et al. Roles for mycobacterial DinB2 in frameshift and substitution mutagenesis. Elife. 2023;12.

13. Kana BD, Abrahams GL, Sung N, Warner DF, Gordhan BG, Machowski EE, et al. Role of the DinB homologs Rv1537 and Rv3056 in Mycobacterium tuberculosis. J Bacteriol. 2010;192(8):2220-7.

14. Ordonez H, Shuman S. Mycobacterium smegmatis DinB2 misincorporates deoxyribonucleotides and ribonucleotides during templated synthesis and lesion bypass. Nucleic Acids Res. 2014;42(20):12722-34.

15. Ordonez H, Uson ML, Shuman S. Characterization of three mycobacterial DinB (DNA polymerase IV) paralogs highlights DinB2 as naturally adept at ribonucleotide incorporation. Nucleic Acids Res. 2014;42(17):11056-70.

16. Warner DF, Ndwandwe DE, Abrahams GL, Kana BD, Machowski EE, Venclovas Č, et al. Essential roles for imuA′- and imuB-encoded accessory factors in DnaE2-dependent mutagenesis in Mycobacterium tuberculosis. Proceedings of the National Academy of Sciences. 2010;107(29):13093-8.

17. Joseph AM, Badrinarayanan A. Visualizing mutagenic repair: novel insights into bacterial translesion synthesis. FEMS Microbiol Rev. 2020;44(5):572-82.

18. Ghodke H, Paudel BP, Lewis JS, Jergic S, Gopal K, Romero ZJ, et al. Spatial and temporal organization of RecA in the Escherichia coli DNA-damage response. eLife. 2019;8:e42761.

19. Goodman MF, McDonald JP, Jaszczur MM, Woodgate R. Insights into the complex levels of regulation imposed on Escherichia coli DNA polymerase V. DNA Repair (Amst). 2016;44:42-50.

20. Friedman N, Vardi S, Ronen M, Alon U, Stavans J. Precise temporal modulation in the response of the SOS DNA repair network in individual bacteria. PLoS Biol. 2005;3(7):e238.

21. Pribis JP, García-Villada L, Zhai Y, Lewin-Epstein O, Wang AZ, Liu J, et al. Gamblers: An Antibiotic-Induced Evolvable Cell Subpopulation Differentiated by Reactive-Oxygen-Induced General Stress Response. Mol Cell. 2019;74(4):785-800.e7.

22. Brzostek A, Płociński P, Minias A, Ciszewska A, Gąsior F, Pawełczyk J, et al. Dissecting the RecA-(In)dependent Response to Mitomycin C in Mycobacterium tuberculosis Using Transcriptional Profiling and Proteomics Analyses. Cells. 2021;10(5):1168.

23. Müller AU, Imkamp F, Weber-Ban E. The Mycobacterial LexA/RecA-Independent DNA Damage Response Is Controlled by PafBC and the Pup-Proteasome System. Cell Rep. 2018;23(12):3551-64.

695 24. Rand L, Hinds J, Springer B, Sander P, Buxton RS, Davis EO. The majority of inducible
696 DNA repair genes in Mycobacterium tuberculosis are induced independently of RecA. Molecular
697 Microbiology. 2003;50(3):1031-42.

698 25. Adefisayo OO, Dupuy P, Nautiyal A, Bean JM, Glickman Michael S. Division of labor
699 between SOS and PafBC in mycobacterial DNA repair and mutagenesis. Nucleic Acids
700 Research. 2021;49(22):12805-19.

701 26. Wipperman MF, Heaton BE, Nautiyal A, Adefisayo O, Evans H, Gupta R, et al.
702 Mycobacterial Mutagenesis and Drug Resistance Are Controlled by Phosphorylation- and
703 Cardiolipin-Mediated Inhibition of the RecA Coprotease. Mol Cell. 2018;72(1):152-61.e7.

704 27. Ragheb MN, Thomason MK, Hsu C, Nugent P, Gage J, Samadpour AN, et al. Inhibiting
705 the Evolution of Antibiotic Resistance. Mol Cell. 2019;73(1):157-65.e5.

706 28. Furukohri A, Goodman MF, Maki H. A dynamic polymerase exchange with Escherichia
707 coli DNA polymerase IV replacing DNA polymerase III on the sliding clamp. J Biol Chem.
708 2008;283(17):11260-9.

709 29. Uphoff S. Real-time dynamics of mutagenesis reveal the chronology of DNA repair and
710 damage tolerance responses in single cells. Proceedings of the National Academy of Sciences.
711 2018;115(28):E6516-E25.

712 30. Jones EC, Uphoff S. Single-molecule imaging of LexA degradation in Escherichia coli
713 elucidates regulatory mechanisms and heterogeneity of the SOS response. Nature
714 Microbiology. 2021;6(8):981-90.

715 31. Pomerantz RT, O'Donnell M. What happens when replication and transcription
716 complexes collide? Cell Cycle. 2010;9(13):2537-43.

717 32. Manina G, Griego A, Singh LK, McKinney JD, Dhar N. Preexisting variation in DNA
718 damage response predicts the fate of single mycobacteria under stress. Embo j.
719 2019;38(22):e101876.

720 33. Lindsey-Boltz LA, Sancar A. The Transcription-Repair Coupling Factor Mfd Prevents and
721 Promotes Mutagenesis in a Context-Dependent Manner. Front Mol Biosci. 2021;8:668290.

722 34. Gessner S, Martin Z, Reiche MA, Santos JA, Dhar N, Dinkele R, et al. The
723 mycobacterial mutasome: composition and recruitment in live cells. bioRxiv.
724 2021:2021.11.16.468908.

725 35. Gordon BR, Imperial R, Wang L, Navarre WW, Liu J. Lsr2 of Mycobacterium represents
726 a novel class of H-NS-like proteins. J Bacteriol. 2008;190(21):7052-9.

727 36. Rock JM, Hopkins FF, Chavez A, Diallo M, Chase MR, Gerrick ER, et al. Programmable
728 transcriptional repression in mycobacteria using an orthogonal CRISPR interference platform.
729 Nature Microbiology. 2017;2(4):16274.

730 37. Minato Y, Gohl DM, Thiede JM, Chacón JM, Harcombe WR, Maruyama F, et al.
731 Genomewide Assessment of Mycobacterium tuberculosis Conditionally Essential Metabolic
732 Pathways. mSystems. 2019;4(4).

733 38. DeJesus MA, Gerrick ER, Xu W, Park SW, Long JE, Boutte CC, et al. Comprehensive
734 Essentiality Analysis of the Mycobacterium tuberculosis Genome via Saturating Transposon
735 Mutagenesis. mBio. 2017;8(1).

736 39. Fudrini Olivencia B, Müller AU, Roschitzki B, Burger S, Weber-Ban E, Imkamp F.
737 Mycobacterium smegmatis PafBC is involved in regulation of DNA damage response. Sci Rep.
738 2017;7(1):13987.

739 40. Murphy KC, Papavinasasundaram K, Sassetti CM. Mycobacterial recombineering.
740 Methods Mol Biol. 2015;1285:177-99.

741 41. Colangeli R, Haq A, Arcus VL, Summers E, Magliozzo RS, McBride A, et al. The
742 multifunctional histone-like protein Lsr2 protects mycobacteria against reactive oxygen
743 intermediates. Proceedings of the National Academy of Sciences. 2009;106(11):4414-8.

744 42. Colangeli R, Helb D, Vilchèze C, Hazbón MH, Lee CG, Safi H, et al. Transcriptional
745 regulation of multi-drug tolerance and antibiotic-induced responses by the histone-like protein
746 Lsr2 in M. tuberculosis. PLoS Pathog. 2007;3(6):e87.

747 43. Kołodziej M, Łebkowski T, Płociński P, Hołówka J, Paściak M, Wojtaś B, et al. Lsr2 and
748 Its Novel Paralogue Mediate the Adjustment of Mycobacterium smegmatis to Unfavorable
749 Environmental Conditions. mSphere. 2021;6(3).

750 44. Bartek IL, Woolhiser LK, Baughn AD, Basaraba RJ, Jacobs WR, Jr., Lenaerts AJ, et al.
751 Mycobacterium tuberculosis Lsr2 is a global transcriptional regulator required for adaptation to
752 changing oxygen levels and virulence. mBio. 2014;5(3):e01106-14.

753 45. Gehrke EJ, Zhang X, Pimentel-Elardo SM, Johnson AR, Rees CA, Jones SE, et al.
754 Silencing cryptic specialized metabolism in Streptomyces by the nucleoid-associated protein
755 Lsr2. eLife. 2019;8:e47691.

756 46. Le Moigne V, Bernut A, Cortès M, Viljoen A, Dupont C, Pawlik A, et al. Lsr2 Is an
757 Important Determinant of Intracellular Growth and Virulence in Mycobacterium abscessus. Front
758 Microbiol. 2019;10:905.

759 47. Wiechert J, Filipchyk A, Hünnefeld M, Gätgens C, Brehm J, Heermann R, et al.
760 Deciphering the Rules Underlying Xenogeneic Silencing and Counter-Silencing of Lsr2-like
761 Proteins Using CgpS of Corynebacterium glutamicum as a Model. mBio. 2020;11(1).

762 48. Kołodziej M, Trojanowski D, Bury K, Hołówka J, Matysik W, Kąkolewska H, et al. Lsr2, a
763 nucleoid-associated protein influencing mycobacterial cell cycle. Scientific Reports.
764 2021;11(1):2910.

765 49. Dulberger CL, Guerrero-Bustamante CA, Owen SV, Wilson S, Wuo MG, Garlena RA, et
766 al. Mycobacterial nucleoid-associated protein Lsr2 is required for productive mycobacteriophage
767 infection. Nature Microbiology. 2023;8(4):695-710.

768 50. Villela AD, Rodrigues VDJ, Pinto AF, Wink PL, Sánchez-Quitian ZA, Petersen GO, et al.
769 Characterisation of iunH gene knockout strain from Mycobacterium tuberculosis. Mem Inst
770 Oswaldo Cruz. 2017;112(3):203-8.

771 51. Owen-Hughes TA, Pavitt GD, Santos DS, Sidebotham JM, Hulton CS, Hinton JC, et al.
772 The chromatin-associated protein H-NS interacts with curved DNA to influence DNA topology
773 and gene expression. Cell. 1992;71(2):255-65.

774 52. Tupper AE, Owen-Hughes TA, Ussery DW, Santos DS, Ferguson DJ, Sidebotham JM,
775 et al. The chromatin-associated protein H-NS alters DNA topology in vitro. Embo j.
776 1994;13(1):258-68.

777 53. Sonnenfield JM, Burns CM, Higgins CF, Hinton JC. The nucleoid-associated protein
778 StpA binds curved DNA, has a greater DNA-binding affinity than H-NS and is present in
779 significant levels in hns mutants. Biochimie. 2001;83(2):243-9.

780 54. Jordi BJAM, Fielder AE, Burns CM, Hinton JCD, Dover N, Ussery DW, et al. DNA
781 Binding Is Not Sufficient for H-NS-mediated Repression ofproU Expression*. Journal of
782 Biological Chemistry. 1997;272(18):12083-90.

783 55. Kouba T, Koval' T, Sudzinová P, Pospíšil J, Brezovská B, Hnilicová J, et al.
784 Mycobacterial HelD is a nucleic acids-clearing factor for RNA polymerase. Nature
785 Communications. 2020;11(1):6419.

786 56. Trojanowski D, Kołodziej M, Hołówka J, Müller R, Zakrzewska-Czerwińska J. Watching
787 DNA Replication Inhibitors in Action: Exploiting Time-Lapse Microfluidic Microscopy as a Tool
788 for Target-Drug Interaction Studies in Mycobacterium. Antimicrob Agents Chemother.
789 2019;63(10).

790 57. Beattie TR, Kapadia N, Nicolas E, Uphoff S, Wollman AJ, Leake MC, et al. Frequent
791 exchange of the DNA polymerase during bacterial chromosome replication. Elife. 2017;6.

792 58. Gordon BRG, Li Y, Wang L, Sintsova A, van Bakel H, Tian S, et al. Lsr2 is a nucleoid-
793 associated protein that targets AT-rich sequences and virulence genes in Mycobacterium
794 tuberculosis. Proceedings of the National Academy of Sciences. 2010;107(11):5154-9.

795 59. Gordon BR, Li Y, Cote A, Weirauch MT, Ding P, Hughes TR, et al. Structural basis for
796 recognition of AT-rich DNA by unrelated xenogeneic silencing proteins. Proc Natl Acad Sci U S
797 A. 2011;108(26):10690-5.

798 60. Báez-Ramírez E, Querales L, Aranaga CA, López G, Guerrero E, Kremer L, et al.
799 Elimination of PknL and MSMEG_4242 in Mycobacterium smegmatis alters the character of the
800 outer cell envelope and selects for mutations in Lsr2. The Cell Surface. 2021;7:100060.

801 61. Tan KW, Pham TM, Furukohri A, Maki H, Akiyama MT. Recombinase and translesion
802 DNA polymerase decrease the speed of replication fork progression during the DNA damage
803 response in Escherichia coli cells. Nucleic Acids Res. 2015;43(3):1714-25.

804 62. Munden A, Rong Z, Sun A, Gangula R, Mallal S, Nordman JT. Rif1 inhibits replication
805 fork progression and controls DNA copy number in Drosophila. eLife. 2018;7:e39140.

806 63. Kobayashi T, Horiuchi T. A yeast gene product, Fob1 protein, required for both
807 replication fork blocking and recombinational hotspot activities. Genes Cells. 1996;1(5):465-74.

808 64. Tsirkas I, Dovrat D, Thangaraj M, Brouwer I, Cohen A, Paleiov Z, et al. Transcription-
809 replication coordination revealed in single live cells. Nucleic Acids Research. 2022;50(4):2143-
810 56.

811 65. Arora K, Whiteford DC, Lau-Bonilla D, Davitt CM, Dahl JL. Inactivation of lsr2 results in a
812 hypermotile phenotype in Mycobacterium smegmatis. J Bacteriol. 2008;190(12):4291-300.

813 66. Kocíncová D, Singh AK, Beretti JL, Ren H, Euphrasie D, Liu J, et al. Spontaneous
814 transposition of IS1096 or ISMsm3 leads to glycopeptidolipid overproduction and affects surface
815 properties in Mycobacterium smegmatis. Tuberculosis (Edinb). 2008;88(5):390-8.

816 67. Alqaseer K, Turapov O, Barthe P, Jagatia H, De Visch A, Roumestand C, et al. Protein
817 kinase B controls Mycobacterium tuberculosis growth via phosphorylation of the transcriptional
818 regulator Lsr2 at threonine 112. Mol Microbiol. 2019;112(6):1847-62.

819 68. Falk T, Mai D, Bensch R, Çiçek Ö, Abdulkadir A, Marrakchi Y, et al. U-Net: deep
820 learning for cell counting, detection, and morphometry. Nature Methods. 2019;16(1):67-70.

821 69. Schindelin J, Arganda-Carreras I, Frise E, Kaynig V, Longair M, Pietzsch T, et al. Fiji: an
822 open-source platform for biological-image analysis. Nature Methods. 2012;9(7):676-82.

823 70. Dragset MS, Ioerger TR, Loevenich M, Haug M, Sivakumar N, Marstad A, et al. Global
824 Assessment of Mycobacterium avium subsp. hominissuis Genetic Requirement for Growth and
825 Virulence. mSystems. 2019;4(6).

826 71. DeJesus MA, Ambadipudi C, Baker R, Sassetti C, Ioerger TR. TRANSIT--A Software
827 Tool for Himar1 TnSeq Analysis. PLoS Comput Biol. 2015;11(10):e1004401.